NASA TECHNICAL NOTE

NASA TN D-5253

ELASTOPLASTIC STRESS-STRAIN BEHAVIOR AT NOTCH ROOTS IN SHEET SPECIMENS UNDER CONSTANT-AMPLITUDE LOADING

by John H. Crews, Jr.

Langley Research Center
Langley Station, Hampton, Va.

NATIONAL AERONAUTICS AND SPACE ADMINISTRATION • WASHINGTON, D. C. • JUNE 1969

ELASTOPLASTIC STRESS-STRAIN BEHAVIOR AT NOTCH ROOTS IN SHEET SPECIMENS UNDER CONSTANT-AMPLITUDE LOADING

By John H. Crews, Jr.

Langley Research Center
Langley Station, Hampton, Va.

NATIONAL AERONAUTICS AND SPACE ADMINISTRATION

For sale by the Clearinghouse for Federal Scientific and Technical Information
Springfield, Virginia 22151 – CFSTI price $3.00

ELASTOPLASTIC STRESS-STRAIN BEHAVIOR AT NOTCH ROOTS IN SHEET SPECIMENS UNDER CONSTANT-AMPLITUDE LOADING

By John H. Crews, Jr.
Langley Research Center

SUMMARY

The adequacy of the modified Stowell and the Neuber equations has been investigated for calculating elastoplastic stress-strain conditions at notch roots for cyclic loading. Edge-notched sheet specimens with elastic stress-concentration factors of 2, 4, and 6 were investigated for several levels of constant-amplitude reversed loading. These specimens were fabricated from 2024-T3 aluminum alloy, SAE 4130 (normalized and stress relieved) steel, and AISI 4130 (normalized) steel. Cyclic stresses and strains were determined experimentally at the notch roots by a companion-specimen method and were compared with notch-root stresses and strains calculated by using both the modified Stowell and the Neuber equations. In general, close correlation was found between calculated and experimental results.

INTRODUCTION

An understanding of the localized stresses at a typical stress raiser is fundamental to the analysis of structural fatigue, since fatigue failures usually originate at stress concentrations. Detailed analyses of these stresses are complex even for elastic behavior and the occurrence of local plasticity usually makes them impractical.

Efforts to provide simpler ways to account for elastoplastic behavior at the points of maximum stress have resulted in two equations for predicting stress and strain. The first of these was developed by Stowell (ref. 1) and modified by Hardrath and Ohman (ref. 2). The second equation was developed by Neuber (ref. 3). Both of these equations can be used to relate stress and strain at the root of a notch to the elastic stress-concentration factor, material properties, and nominal stress. These equations have been altered slightly for fatigue applications (for example, refs. 4, 5, and 6) and used to estimate stress and strain histories at notch roots for cyclic loading. However, the accuracy of these equations in describing cyclic conditions at a notch root has not been studied beyond the first cycle.

The present investigation was undertaken to assess the adequacy of these two equations for application to cyclic loading. This study was carried out in three parts. In the first part, cyclic stresses and strains at notch roots, referred to herein as "local" stresses and strains, were determined experimentally by a companion-specimen technique. In the second part of this study, local stresses and strains were calculated by using both the modified Stowell equation and the Neuber equation and compared with experimental results. In the third part, local stresses were determined from a cyclic stress-strain curve and compared with stabilized local stresses found in the first part of this study.

SYMBOLS

The units used for the physical quantities defined in this paper are given both in U.S. Customary Units and in the International System of Units (SI) (ref. 7). Factors relating these two systems of units are presented in the appendix.

a notch depth, in. (m)

E Young's modulus, ksi (GN/m^2)

E_s secant modulus corresponding to local stress at notch root, ksi (GN/m^2)

$E_{s,i} \equiv \Delta\sigma_i / \Delta\epsilon_i$

h length of test section for unnotched specimen, in. (m)

K_{exp} experimental elastic stress-concentration factor

K_T theoretical elastic stress-concentration factor

K_ϵ strain-concentration factor

K_σ stress-concentration factor

N cycles

R ratio of S_{min}/S_{max}

S nominal net-section stress, ksi (MN/m^2)

S_{max} maximum nominal net-section stress, ksi (MN/m^2)

S_{min} minimum nominal net-section stress, ksi (MN/m^2)

ΔS monotonic nominal stress excursion, ksi (MN/m^2)

ΔS_i ith monotonic nominal stress excursion, ksi (MN/m^2)

ϵ local strain at notch root

$\Delta\epsilon_i$ monotonic local strain excursion corresponding to ΔS_i

ρ notch root radius, in. (m)

σ local stress at notch root, ksi (MN/m^2)

$\Delta\sigma$ monotonic local stress excursion, ksi (MN/m^2)

$\Delta\sigma_i$ monotonic local stress excursion corresponding to ΔS_i, ksi (MN/m^2)

PART 1 – EXPERIMENTAL STUDY OF LOCAL STRESS AND STRAIN

The calculation of local stresses directly from measured local strains is complicated by the history dependence of local elastoplastic stress-strain behavior and by cyclic variations in stress-strain properties. To avoid these problems, local stresses were determined in this study by a companion-specimen method. This method, other experimental details, and results are presented and discussed in the following sections.

Experimental Apparatus and Procedure

Specimens.- Tests were conducted with edge-notched sheet specimens. Dimensions for these specimens are given in figure 1 and were selected for elastic stress-concentration factors of 2, 4, and 6 (ref. 8). Attention was restricted to the point of maximum stress concentration, and for each specimen configuration, this point was located at the notch root. Because a state of plane stress existed in the vicinity of the notch root, this point on the boundary of the notch was in a state of uniaxial stress. Three materials were used: 2024-T3 aluminum alloy, SAE 4130 (normalized and stress relieved) steel, and AISI 4130 (normalized) steel. Pairs of notched and companion specimens (fig. 1) were cut from adjacent positions in the sheet stock and were oriented so that loading was parallel to the rolling direction of the sheet stock.

Companion-specimen method.- The cyclic local stress and strain at notch roots were determined by a companion-specimen method. For a given test, local strain-gage readings were taken at the notch root at discrete loading intervals. This sequence of strain-gage readings was reproduced in strain gages on an unnotched companion specimen to determine the stress corresponding to each strain level. Because the local point at the notch root and the companion specimen are both in uniaxial states of stress, the stress sequence obtained in this manner is a close approximation to the local stress at the notch root.

Instrumentation.- Strains at the notch roots were measured with foil strain gages cemented to the edge of the specimen. In the tests of $K_T = 2$ specimens, strain gages with a gage length of 0.062 in. (1.6 mm) were used, and in tests of $K_T = 4$ and $K_T = 6$ specimens, strain gages with a gage length of 0.015 in. (0.4 mm) were used. In all tests, pairs of gages, one at each notch root or one on each face of the companion specimen, were connected in series to indicate the average strains. To minimize the effects of strain-gage zero-shift errors (ref. 9) on the local stress results, the pair of strain gages used on a given companion specimen was of the same type and lot number as the pair used on the corresponding notched specimen.

Specimen loading.- The notched specimens were subjected to full cycles of equal tensile and compressive loading. Loading was applied incrementally with local strain measurements being made at each interval. The maximum values of nominal stress S_{max} were selected to give values of $K_T S_{max}$ of 60, 100, and 150 ksi (413, 689, and 1030 MN/m^2).

Companion tests were conducted with a servo-controlled hydraulic test machine. Loading on the companion specimen was carefully varied to reproduce the sequence of strain-gage readings recorded for the notch root. The load corresponding to each strain-gage reading was recorded and local stresses were calculated directly from the resulting load sequence. Guide plates were used with both the notched and companion specimens to prevent buckling during compressive loading.

Experimental elastic stress-concentration factor.- Experimental elastic stress-concentration factors K_{exp} were determined for each test condition. During the initial stage of loading, local strain readings were recorded at approximately 10 nominal stress levels throughout the range of local elastic behavior. The local stress corresponding to each of these nominal stresses was found from the companion-specimen tests. The factor K_{exp} was calculated for each nominal stress level and an average of these values was taken as the K_{exp} for each test.

Experimental Results

Elastic stress-concentration factors.- The notches used in the present study were machined with parallel sides and semicircular roots. For the same depth and root radius this type of notch is somewhat sharper than a corresponding hyperbolic notch used to derive K_T (ref. 8). Therefore, the K_{exp} values should be higher than the K_T values found by using the theory in reference 8. The K_{exp} and the corresponding K_T values given in table I differ by 4 to 14 percent.

First-cycle stress-strain curves.- To demonstrate the effects of nominal stress range on first-cycle stress and strain, a set of stress-strain curves from companion specimens for various S_{max} is shown together in figures 2 to 6 for each combination of material and specimen configuration. Residual stress-strain values are represented by solid symbols and the loci of these points as influenced by nominal stress are shown as dashed curves. These points represent stress and strain for zero load on the notched specimen.

For $K_T = 2$ (fig. 2) the loci of half-cycle and full-cycle residual stresses and strains were approximately antisymmetrical about the origin. For $K_T = 4$ and 6 (figs. 3 and 4) the residual stresses were also nearly antisymmetrical, but the residual strains were not. The full-cycle residual strains were generally smaller than the corresponding half-cycle values. Thus, the antisymmetry of the loci displayed in figure 2 and also reported in reference 10 is not generally characteristic of residual stress-strain behavior for completely reversed loading.

With the exception of a single test with $K_T = 2$, 2024-T3, and $S_{max} = 40$ ksi (276 MN/m^2), all the tests were performed with $K_T S_{max} = 60$, 100, or 150 ksi (413, 689, or 1030 MN/m^2) to facilitate comparisons between local stress and strain for different notch configurations. Maximum, minimum, and residual values of stress and strain from figures 2, 3, and 4 are listed in table I. Maximum and minimum stresses during the first loading cycle for different K_T values but for the same $K_T S_{max}$ level were nearly equal. However, residual stresses were larger for higher K_T levels; this was due in part to the larger differences between $K_{exp} S_{max}$ and $K_T S_{max}$ for higher K_T values. Local strains had slightly smaller maximum values and ranges for higher K_T levels than for lower K_T levels.

The local stress-strain curves for the 4130 steel specimens (figs. 5 and 6) were obtained by using two different heat treatments for this material. The material from which the $K_T = 2$ specimen was made had been normalized and stress relieved. The material used for the $K_T = 4$ specimens had only been normalized. As a result, the stress-strain curves for the two steels (figs. 5 and 6) were quite different, which precluded a comparison of results for 4130 specimens on a $K_T S_{max}$ basis. Nevertheless,

these results were useful in the evaluation of the analytical method presented in the second part of this study.

Local stresses during repeated cycles.- The symbols in figures 7, 8, and 9 represent maximum, minimum, and residual stresses found during the first 30 cycles of loading on 2024-T3 specimens having equal $K_T S_{max}$ values. Similar experimental results are plotted in figure 10 for 4130 steel. At a $K_T S_{max}$ value of 60 ksi (413 MN/m^2), the measured local stresses (data points in fig. 7) for specimens having various K_T values were very nearly equal over the entire cyclic history. At a $K_T S_{max}$ value of 100 ksi (689 MN/m^2) (fig. 9), the agreement for the various K_T values is not as good. Some of the scatter can be attributed to the differences between $K_{exp} S_{max}$ values noted in table I for this series of tests. In general, the cyclic stress levels are approximately equal at constant $K_T S_{max}$ values for 2024-T3 aluminum alloy.

In figures 7, 8, and 9 an increase in stress range (cyclic strain hardening) occurred during the first 10 cycles after which the local stress level stabilized. Since the local behavior was nearly elastic during unloading for all $K_T S_{max}$ values (see figs. 2, 3, and 4), the residual stresses experienced decreases in magnitude which were nearly equal to the corresponding increases in maximum and minimum local stresses.

Results from a single test with a 4130 steel specimen are shown in figure 10. In this test minimum stresses remained unchanged and the maximum stress decreased slightly, which is an indication of the cyclic softening behavior reported in reference 11 for this material.

PART 2 – CALCULATION OF LOCAL STRESS AND STRAIN

The companion-specimen method explained in the previous section was based upon the simulation of local cyclic stress-strain behavior of notched specimens with unnotched specimens. Unnotched uniaxial specimens were cycled between experimental local strain limits found from the notched specimens. The procedure described in this section was based upon a similar simulation of local cyclic conditions, but the limits for cycling the unnotched specimens were calculated. Two equations are currently available for calculating the limiting conditions for local stress and strain. These relationships are the modified Stowell and the Neuber equations.

Modified Stowell Equation for Local Stress and Strain

Stowell (ref. 1) investigated local elastoplastic stress and strain behavior in an infinite sheet containing a circular hole subjected to uniform tension. To account for local plasticity, Stowell introduced the ratio E_s/E_∞ into the elastic solution, where

E_S is the secant modulus corresponding to the local stress and E_∞ is the secant modulus corresponding to the uniform stress remote from the hole.

The stress-concentration factor for elastoplastic behavior then becomes (based on ref. 1)

$$K_\sigma = 1 + 2\frac{E_S}{E_\infty}$$

Hardrath and Ohman (ref. 2) modified this relationship through the introduction of K_T and demonstrated that

$$K_\sigma = 1 + (K_T - 1)\frac{E_S}{E} \tag{1}$$

was generally applicable for stress concentrations in sheet specimens under loading when the nominal stress is still elastic.

Equation (1) was extended to include cases of cyclic loading in reference 9 and rewritten as

$$K_\sigma = \frac{\Delta\sigma_i}{\Delta S_i} = 1 + (K_T - 1)\frac{E_{S,i}}{E} \tag{2}$$

where $\Delta\sigma_i$ and $E_{S,i}$ are the monotonic local stress excursion and the corresponding secant modulus resulting from the ith monotonic nominal stress variation ΔS_i.

For the purpose of establishing the extreme values of local stress and strain for a given cycle of nominal loading, equation (2) can be rewritten in terms of the variables $\Delta\sigma_i$ and $\Delta\epsilon_i$ by taking account of the fact that $E_{S,i} \equiv \Delta\sigma_i/\Delta\epsilon_i$. The resulting equation is

$$\Delta\sigma_i = \frac{\Delta\epsilon_i\,\Delta S_i}{\Delta\epsilon_i - (K_T - 1)\frac{\Delta S_i}{E}} \tag{3}$$

This form of the modified Stowell equation was used in the present study.

Neuber Equation for Local Stress and Strain

In reference 3 Neuber considered the problem of prismatical bodies containing stress concentrations under shear strain. From this study Neuber concluded that the geometric mean of the stress- and strain-concentration factors is equal to the elastic stress-concentration factor. This may be expressed as

$$K_\sigma K_\epsilon = K_T^2$$

For use in the present study, this equation can be rewritten in terms of $\Delta\sigma_i$ and $\Delta\epsilon_i$ for elastic nominal loading to give

$$\Delta\sigma_i = \frac{\left(K_T\,\Delta S_i\right)^2}{\Delta\epsilon_i E} \tag{4}$$

Procedure for Calculating Local Stress and Strain

The procedure used in calculating local stress and strain can be explained with figure 11(a), which shows a typical first cycle of nominal stress for which local behavior was sought. This cycle has been divided into monotonic excursions of nominal stress and each excursion has been labeled.

To illustrate the procedure, equation (4) was evaluated for a given K_T, E, and ΔS_1 and plotted in the first quadrant of figure 11(b). The resultant dashed curve represents the locus of maximum local stress and strain. An unnotched specimen was loaded in uniaxial tension to generate the curve OA. The intersection, point A, represents the only solution to equation (4) consistent with the material behavior characterized by OA and, as a result, determines the estimated values of $\Delta\sigma_1$ and $\Delta\epsilon_1$ corresponding to ΔS_1.

For the second excursion ΔS_2, point A was taken as the initial state for local stress and strain. Accordingly, equation (4) was evaluated for ΔS_2 and plotted with $\Delta\sigma_2$ and $\Delta\epsilon_2$ referenced to point A. The unnotched specimen was unloaded from A and loaded into compression until the stress-strain curve intersected this curve for equation (4) at point C. This intersection point represents the estimated minimum values for local stress and strain corresponding to the minimum stress in figure 11(a). The intermediate point B for this excursion of local behavior represents the residual stress-strain state and was found by plotting equation (4) relative to A corresponding to removal of ΔS_1 from the notched specimen. Point D was found in a similar manner to complete the first cycle of local behavior. This procedure was repeated to estimate the local stress and strain for succeeding cycles.

Discussion of Results

As previously mentioned, the experimental stress-concentration factors found in this study are slightly higher than the values calculated by the Neuber theory from reference 8 for hyperbolic notches. To eliminate errors due to these discrepancies in elastic stress-concentration factors, the experimental values of stress-concentration factor

K_{exp} were used in the equations to calculate local stress and strain behavior. Values of $E = 10\ 400$ ksi (71.7 GN/m^2) and $E = 29\ 200$ ksi (201 GN/m^2) were used, respectively, for the aluminum and steel specimens.

Local stress-strain curves for the first loading cycle.- Estimated local stress-strain curves for the first cycle of reversed loading are presented in figures 12(a) to 12(l). These curves are plotted separately for each specimen and nominal stress level. For comparison the experimental curves from figures 2 to 6 are also plotted in figure 12.

For $K_T = 2$ the local stress-strain curves found by using the Neuber equation (eq. (4)) were nearly the same as the corresponding experimental curves. However, the local stress and strain estimated by use of the modified Stowell equation (eq. (3)) were noticeably farther into the plastic range than the experimental results for this K_T value. For the higher K_T levels this trend was reversed. The estimated stresses and strains from the Neuber equation were larger than the corresponding Stowell results and, in general, the experimental curves were between the two estimated curves.

This behavior can be explained with the aid of figure 13 in which the Neuber and the modified Stowell equations are plotted for $E = 10\ 400$ ksi (71.7 GN/m^2) and $K_T S_{max} = 100$ ksi (689 MN/m^2). The monotonic stress-strain curve for 2024-T3 is also plotted in figure 13 and the intersections of the Neuber and Stowell curves with this stress-strain curve provide estimates of local stress and strain. The plot of the Neuber equation is a single curve and, as a result, yields a single estimate of local behavior. However, the Stowell equation yields a separate curve for each nominal stress value. The estimated local stress and strain for $K_T = 2$ from the Stowell equation are larger than the corresponding values found with the Neuber equation. For $K_T = 4$ and 6, the estimated local stresses and strains from the Stowell equation are smaller than the Neuber values.

In general, because the Neuber and the Stowell curves cross (for example, point A, fig. 13), the relative magnitudes of the estimated local strains found by use of the two equations depend upon the stress-strain curve. If the stress-strain curve intersects these curves above their common point (as in fig. 13), the Stowell estimate of local stress is less than the corresponding Neuber estimate. Conversely, for stress-strain curves that lie below this intersection point, the Neuber estimates are smaller. As a result of this dependence on the stress-strain curves, the relative magnitudes of estimated maximum local conditions shown in figure 12 should not be taken as being generally representative for all materials. The comparisons of estimated local results for the two methods must be restricted to the values of K_T and S_{max} and materials considered in this study.

An overall evaluation of the estimated and the experimental curves in figure 12 yields no definite superiority of one equation over the other. However, a comparison of the maximum local strains listed in table I shows that these strains are nearly constant for a given $K_T S_{max}$ level. Since the Neuber equation yields a single estimate of strain for a given $K_T S_{max}$, the Neuber equation appears to be more nearly representative of this feature of local behavior than the Stowell equation. Nevertheless, for the determination of local stresses, either equation provides a reasonable estimate of local stress and strain at notches.

Local stress during repeated cycles.- The procedure used to estimate the first-cycle behavior was repeatedly applied to determine the local stress-strain behavior for the first 30 loading cycles. The maximum, minimum, and residual stresses found by using the Neuber equation with this procedure are shown in figures 7 and 9 for 2024-T3 as solid curves. For each $K_T S_{max}$ level an average value was taken for $K_{exp} S_{max}$ and this value was used in equation (4). For both $K_T S_{max}$ = 60 and 100 ksi (413 and 689 MN/m^2) the estimated stress ranges increased and reached a stabilized level in about 15 cycles. The experimental and calculated local stress histories were in reasonable agreement (figs. 7 and 9). The local strain histories corresponding to these estimated local stresses are shown in figure 14. The estimated strain ranges decreased rapidly during the first 5 cycles and at a slower rate during the remaining 25 cycles. Because of the zero shifts experienced by the strain gages, local strain histories were not determined experimentally and are not compared here.

PART 3 – CALCULATION OF STABILIZED LOCAL STRESS

In reference 10, stabilized local stresses were used to predict fatigue lives for notched specimens from S-N curves found with unnotched specimens. However, the methods used in reference 10 and the first two phases of the present study were based upon cycle-by-cycle determinations of local behavior. In an effort to develop a more direct and efficient procedure for calculating local stress, methods from the second part of this study were applied together with a cyclic stress-strain curve which characterized the stabilized material behavior. Stabilized local stress and strain were calculated by this approach for the R = -1 loading conditions considered in this study. Calculated local stresses from this part of the study were compared with the experimental local stresses from the first part.

Procedure

The extreme values of stabilized local stress and strain were calculated as indicated in figure 15. The cyclic stress-strain curve (solid curve) shown in this figure was developed by cycling unnotched specimens (fig. 1(b)) under constant-amplitude strain

control until the corresponding stress ranges stabilized (symbols). Equation (4) was used to calculate the extreme values of local stress and strain (dashed curves) by using the average value of $K_{exp}S_{max}$ from table I corresponding to each K_TS_{max} level. Since the local maximum and minimum stresses in figures 7, 8, and 9 were nearly symmetrical with respect to zero stress, the dashed curves for equation (4) were positioned to intersect the cyclic stress-strain curve at symmetrical values of local stress. This symmetry was obtained by first assuming an estimate for maximum stabilized local stress and then plotting equation (4) relative to this stress value on the cyclic stress-strain curve. The intersection of this curve for equation (4) (see the third quadrant) with the cyclic stress-strain curve was the initial estimate for the minimum stabilized local stress and strain. If this estimate for minimum stabilized local stress was not equal in magnitude to the assumed maximum stabilized local stress, a new maximum stress level was selected and the previous procedure repeated to find a second estimate of minimum stabilized local stress. This entire procedure was continued until the assumed symmetry of maximum and minimum stabilized local stresses was obtained. The curves for equation (4) corresponding to the final estimates are shown in figure 15. In addition, the curves for equation (4) relative to the minimum points are shown in the first quadrant.

The stabilized residual conditions were calculated by combining these estimates of maximum and minimum conditions with the estimates of stabilized unloading ranges shown in figure 16. The stabilized hysteresis loops in this figure were found from the strain-controlled tests used to establish the cyclic stress-strain curve in figure 15. These loops are superimposed with a common minimum point for convenience. Equation (4) was plotted for average values of $K_{exp}S_{max}$ corresponding to unloading the notched specimens. The intersections of these dashed curves and the stabilized loops represent estimates for the stabilized ranges of local stress and strain during unloading from compression. By combining these estimates with the corresponding estimates of stabilized minimum local stress from figure 15, the estimated values of stabilized full-cycle residual stresses were obtained. Because of the assumed local stress symmetry these values were also estimates for the stabilized half-cycle residual stresses.

Discussion of Results

To evaluate the accuracy of these estimates of stabilized local stress, dashed lines were placed in figures 7, 8, and 9 at each estimated stress level. The experimental results and the estimates of stabilized stresses correlated better for high K_TS_{max} levels. This trend could be interpreted as an indication that local stress stabilization had not occurred at the end of 30 cycles for the lower K_TS_{max} values. This interpretation would be consistent with the observation (ref. 11) that stabilization occurs more rapidly at higher levels of cyclic strain. However, in general, the experimental and estimated results from figures 7, 8, and 9 were in reasonable agreement.

CONCLUSIONS

The adequacy of the modified Stowell and the Neuber equations has been investigated for calculating elastoplastic stress-strain conditions at notch roots for cyclic loading. Edge-notched sheet specimens of 2024-T3 aluminum alloy and 4130 steel were studied under reversed constant-amplitude loading and results support the following conclusions:

1. For specimens which had elastic stress-concentration factors of approximately 2, 4, and 6, the local stress-strain behavior was essentially the same for constant values of the product of maximum nominal stress S_{max} and elastic stress-concentration factor K_T.

2. Stabilization of local stresses appeared to occur in approximately 15 cycles of reversed loading for 2024-T3. The local stress range increased and the local strain range decreased during the stabilization phase. Half-cycle and full-cycle residual stresses decreased in magnitude as the maximum and minimum stresses increased.

3. In a single test with 4130 steel, the local stress range decreased slightly but did not stabilize in 30 cycles of reversed loading.

4. Estimates of local stress and strain made by using the modified Stowell equation and the Neuber equation were good approximations to experimental results for the first cycle of reversed loading. For a constant $K_T S_{max}$ value, the modified Stowell equation yielded estimates of local stress and strain that varied inversely with K_T. The Neuber equation yielded a single estimate of local stress and strain for a given $K_T S_{max}$.

5. Estimates of local cyclic stress found for 2024-T3 by repeatedly applying the Neuber equation in a cycle-by-cycle manner correlated well with experimental results during the first 30 cycles of loading.

6. Estimates of stabilized local stress for 2024-T3 calculated by using the Neuber equation and a cyclic stress-strain curve for this material were close approximations to experimental results for high $K_T S_{max}$ values.

Langley Research Center,
National Aeronautics and Space Administration,
Langley Station, Hampton, Va., April 10, 1969,
126-14-03-09-23.

APPENDIX

CONVERSION OF U.S. CUSTOMARY UNITS TO SI UNITS

The International System of Units (SI) was adopted by the Eleventh General Conference on Weights and Measures, Paris, October 1960, in Resolution No. 12 (ref. 7). Conversion factors for the units used herein are given in the following table:

Physical quantity	U.S. Customary Unit	Conversion factor (*)	SI Unit
Length	in.	0.0254	meter (m)
Stress	psi = lbf/in^2	6.895×10^3	newtons per square meter (N/m^2)

*Multiply value given in U.S. Customary Unit by conversion factor to obtain equivalent value in SI Units.

Prefixes to indicate multiple of units are as follows:

Prefix	Multiple
mega (M)	10^6
giga (G)	10^9
centi (c)	10^{-2}
milli (m)	10^{-3}

REFERENCES

1. Stowell, Elbridge Z.: Stress and Strain Concentration at a Circular Hole in an Infinite Plate. NACA TN 2073, 1950.

2. Hardrath, Herbert F.; and Ohman, Lachlan: A Study of Elastic and Plastic Stress Concentration Factors Due to Notches and Fillets in Flat Plates. NACA Rep. 1117, 1953. (Supersedes NACA TN 2566.)

3. Neuber, H.: Theory of Stress Concentration for Shear-Strained Prismatical Bodies With Arbitrary Nonlinear Stress-Strain Law. Trans. ASME, Ser. E: J. Appl. Mech., vol. 28, no. 4, Dec. 1961, pp. 544-550.

4. Peterson, R. E.: Fatigue of Metals. Part 3 – Engineering and Design Aspects. Mater. Res. Stand., vol. 3, no. 2, Feb. 1963, pp. 122-129.

5. Dolan, T. J.: Nonlinear Response Under Cyclic Loading Conditions. Developments in Mechanics, Vol. 3, Pt. 1, T. C. Huang and M. W. Johnson, Jr., eds., John Wiley & Sons, Inc., 1965, pp. 3-21.

6. Manson, S. S.; and Hirschberg, M. H.: Crack Initiation and Propagation in Notched Fatigue Specimens. Proceedings of the First International Conference on Fracture, Vol. 1, T. Yokobori, T. Kawasaki, and J. L. Swedlow, eds., Jap. Soc. Strength Fracture Mater., c.1966, pp. 478-498.

7. Comm. on Metric Pract.: ASTM Metric Practice Guide. NBS Handbook 102. U.S. Dep. Com., Mar. 10, 1967.

8. Neuber, Heinz: Theory of Notch Stresses: Principles for Exact Calculation of Strength With Reference to Structural Form and Material. AEC-tr-4547, U.S. At. Energy Com., 1961.

9. Krempl, Erhard: Evaluation of High-Elongation Foil Strain Gages for Measuring Cyclic Plastic Strains. Exp. Mech., vol. 8, no. 8, Aug. 1968, pp. 19N-26N.

10. Crews, John H., Jr.: Local Plastic Stresses in Sheet Aluminum-Alloy Specimens With Stress-Concentration Factor of 2 Under Constant-Amplitude Loading. NASA TN D-3152, 1965.

11. Smith, Robert W.; Hirschberg, Marvin H.; and Manson, S. S.: Fatigue Behavior of Materials Under Strain Cycling in Low and Intermediate Life Range. NASA TN D-1574, 1963.

TABLE I.- EXPERIMENTAL RESULTS FOR FIRST LOADING CYCLE

(a) U.S. Customary Units

$K_T S_{max}$, ksi	Material	S_{max}, ksi	K_T	K_{exp}	$K_{exp} S_{max}$, ksi	Local stress and strain							
						Maximum		Half-cycle residual		Minimum		Full-cycle residual	
						σ, ksi	ϵ, %	σ, ksi	ϵ, %	σ, ksi	ϵ, %	σ, ksi	ϵ, %
60	2024-T3	30	2	2.12	63.6	51.4	0.671	-12.8	0.048	-49.6	-0.727	15.5	-0.118
60	2024-T3	15	4	4.39	65.9	51.7	.652	-13.8	.028	-46.8	-.715	18.0	-.107
60	2024-T3	10	6	6.68	66.8	51.8	.661	-14.0	.028	-48.5	-.676	16.8	-.065
80	2024-T3	40	2	2.12	84.8	53.9	1.27	-27.8	.422	-57.9	-1.15	25.6	-.326
100	2024-T3	50	2	2.09	104.5	57.6	1.91	-37.3	.828	-65.8	-1.90	35.6	-.849
100	2024-T3	25	4	4.46	111.5	55.5	1.79	-40.8	.632	-61.0	-1.36	39.6	-.262
100	2024-T3	16.7	6	6.82	113.9	57.6	1.65	-43.0	.486	-63.8	-1.48	41.2	-.346
150	2024-T3	37.5	4	4.54	170.2	61.1	3.72	-54.7	1.86	-72.7	-2.35	58.0	-.584
150	2024-T3	25	6	6.77	169.2	62.7	3.56	-56.2	1.64	-74.2	-2.45	58.5	-.654
100	[a]4130	50	2	2.08	104.0	88.9	.418	-14.6	.042	-83.3	-.491	20.9	-.117
100	[b]4130	25	4	4.50	112.5	78.4	.460	-27.9	.067	-82.0	-.451	27.2	-.065
150	[b]4130	37.5	4	4.56	171.0	81.8	1.04	-51.6	.361	-86.6	-.911	50.8	-.268

[a]SAE 4130 (normalized and stress relieved).

[b]AISI 4130 (normalized).

TABLE I.- EXPERIMENTAL RESULTS FOR FIRST LOADING CYCLE – Concluded

(b) SI Units

$K_T S_{max}$, MN/m^2	Material	S_{max}, MN/m^2	K_T	K_{exp}	$K_{exp} S_{max}$, MN/m^2	Local stress and strain							
						Maximum		Half-cycle residual		Minimum		Full-cycle residual	
						σ, MN/m^2	ϵ, %	σ, MN/m^2	ϵ, %	σ, MN/m^2	ϵ, %	σ, MN/m^2	ϵ, %
413	2024-T3	207	2	2.12	439	354	0.671	-88	0.048	-342	-0.727	107	-0.118
413	2024-T3	103	4	4.39	454	356	.652	-95	.028	-323	-.715	124	-.107
413	2024-T3	69	6	6.68	461	357	.661	-97	.028	-334	-.676	116	-.065
552	2024-T3	276	2	2.12	585	372	1.27	-192	.422	-399	-1.15	177	-.326
689	2024-T3	345	2	2.09	721	397	1.91	-257	.828	-454	-1.90	245	-.849
689	2024-T3	172	4	4.46	769	383	1.79	-281	.632	-421	-1.36	273	-.262
689	2024-T3	115	6	6.82	785	397	1.65	-296	.486	-440	-1.48	284	-.346
1030	2024-T3	259	4	4.54	1174	421	3.72	-377	1.86	-501	-2.35	400	-.584
1030	2024-T3	172	6	6.77	1167	432	3.56	-387	1.64	-512	-2.45	403	-.654
689	[a]4130	345	2	2.08	717	613	.418	-101	.042	-574	-.491	144	-.117
689	[b]4130	172	4	4.50	776	541	.460	-192	.067	-565	-.451	188	-.065
1030	[b]4130	259	4	4.56	1179	564	1.04	-356	.361	-597	-.911	350	-.268

[a]SAE 4130 (normalized and stress relieved).

[b]AISI 4130 (normalized).

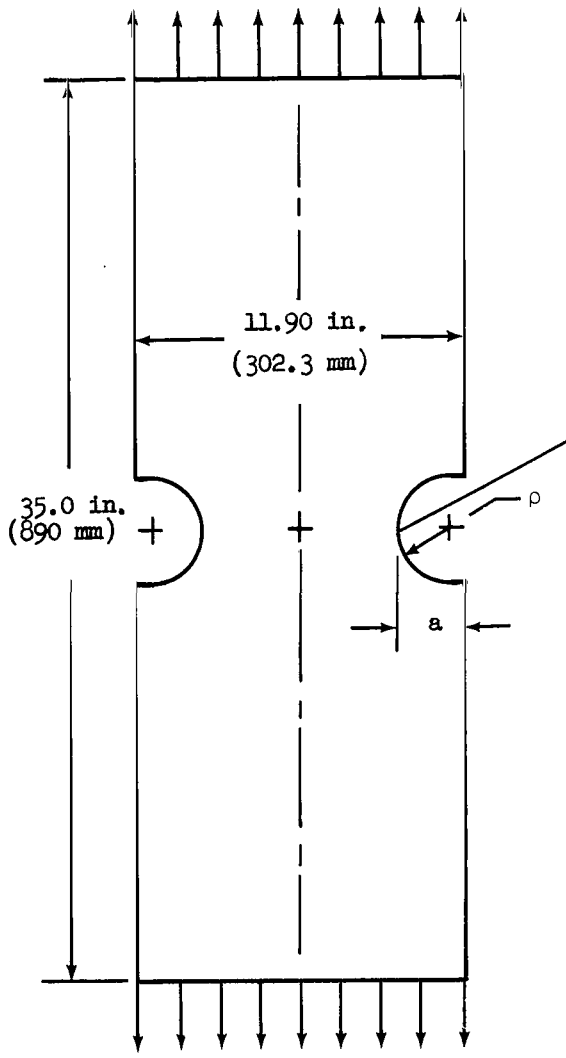

(a) Notched specimen.

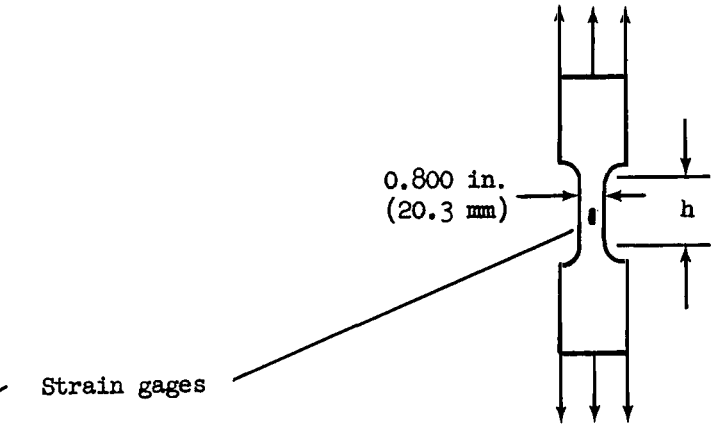

(b) Companion specimen.

K_T	Material	a, in. (mm)	ρ, in. (mm)	h, in. (mm)	Sheet thickness, in. (mm)
2	2024–T3	2.028 (51.51)	1.672 (42.47)	5.00 (127)	0.162 (4.11)
2	4130	2.028 (51.51)	1.672 (42.47)	2.00 (50.8)	0.082 (2.08)
4	2024–T3	1.965 (49.91)	0.300 (7.62)	2.00 (50.8)	0.156 (3.96)
4	4130	1.965 (49.91)	0.300 (7.62)	2.00 (50.8)	0.187 (4.75)
6	2024–T3	2.000 (50.80)	0.122 (3.10)	2.00 (50.8)	0.156 (3.96)

Figure 1.- Specimen dimensions and instrumentation.

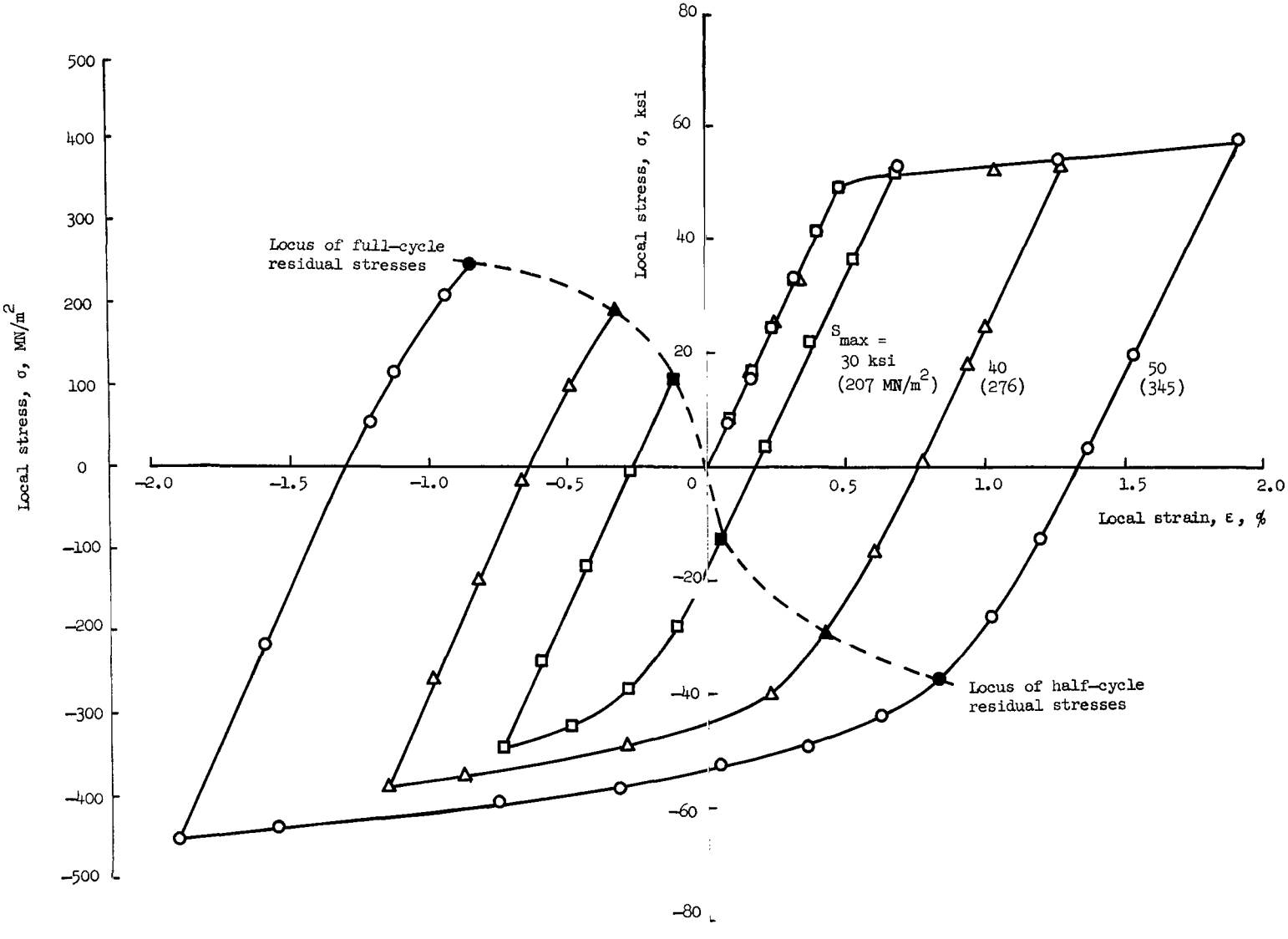

Figure 2.- Local stress-strain curves for first cycle. K_T = 2; 2024-T3; R = -1. Solid symbols represent residual stress-strain values.

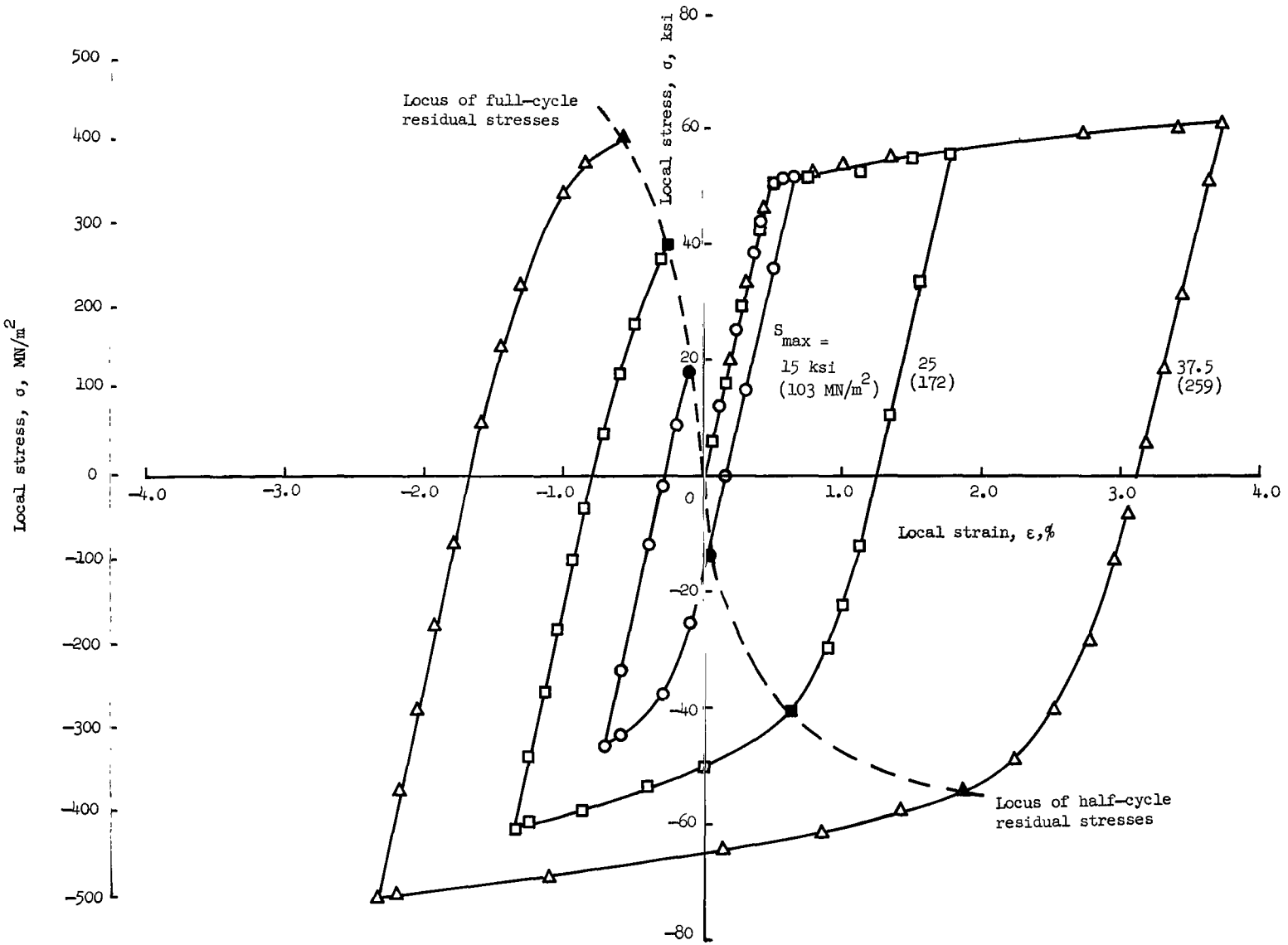

Figure 3.- Local stress-strain curves for first cycle. K_T = 4; 2024-T3; R = -1. Solid symbols represent residual stress-strain values.

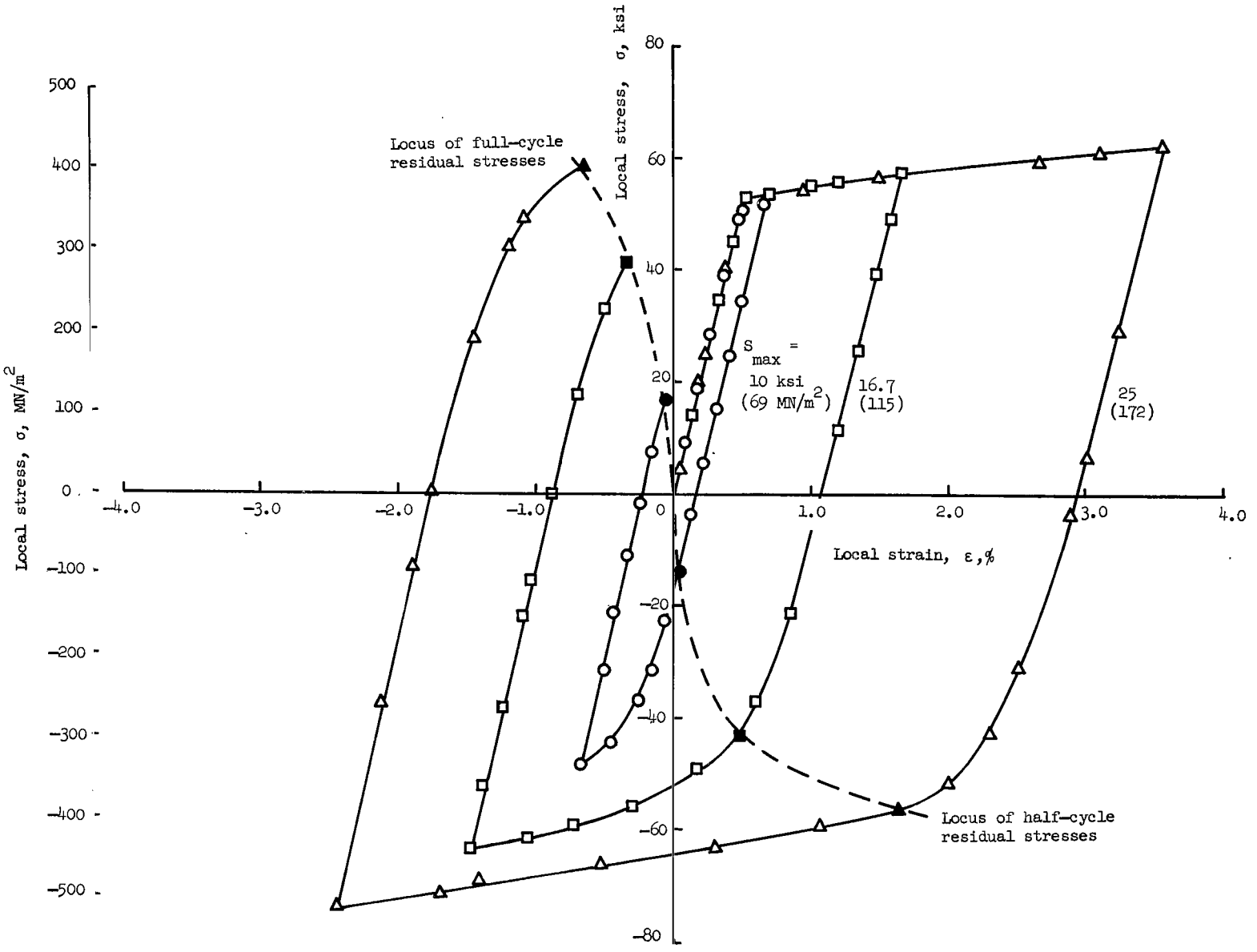

Figure 4.- Local stress-strain curves for first cycle. K_T = 6; 2024-T3; R = -1. Solid symbols represent residual stress-strain values.

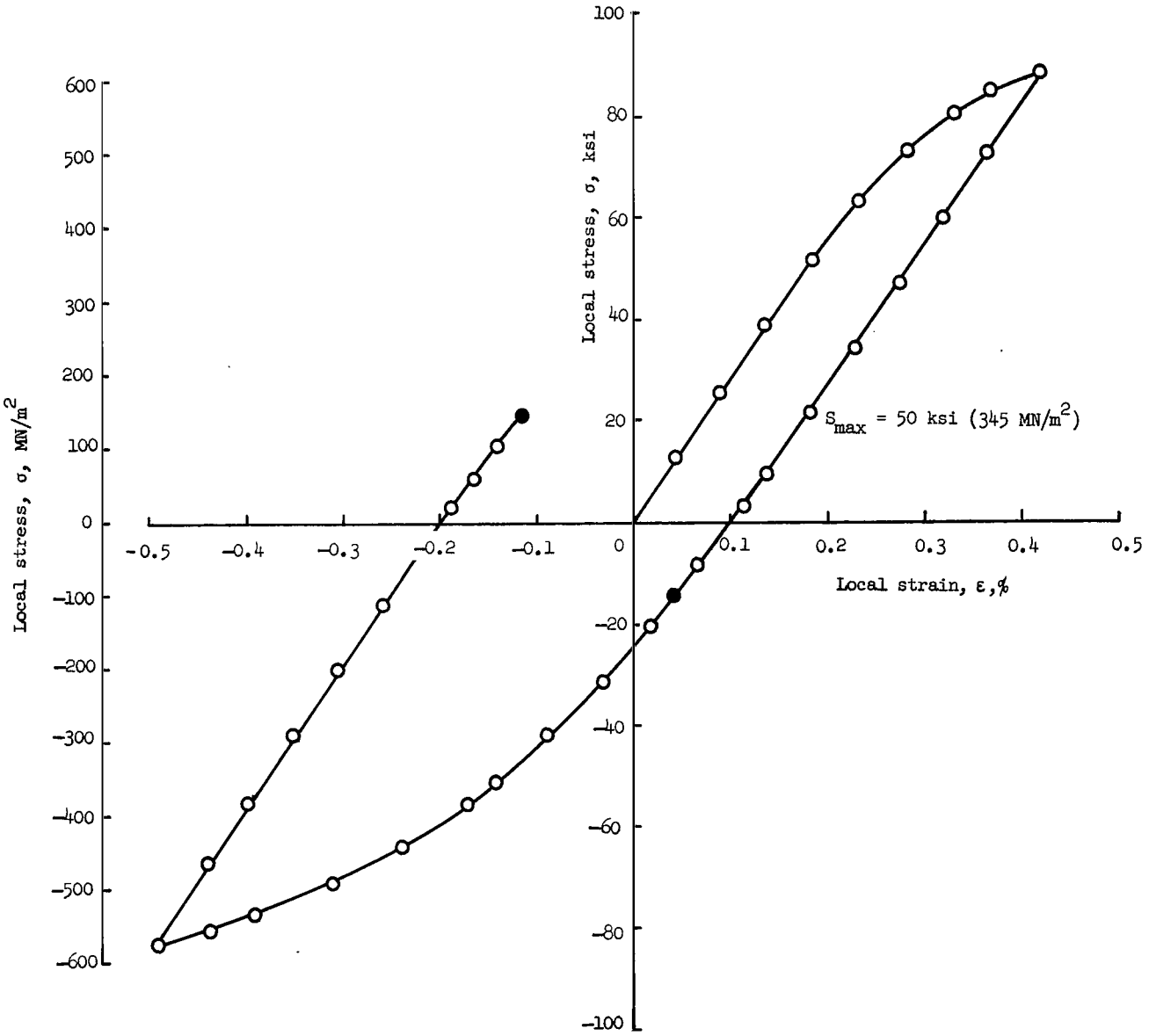

Figure 5.- Local stress-strain curve for first cycle. K_T = 2; SAE 4130 (normalized and stress relieved); R = -1. Solid symbols represent residual stress-strain values.

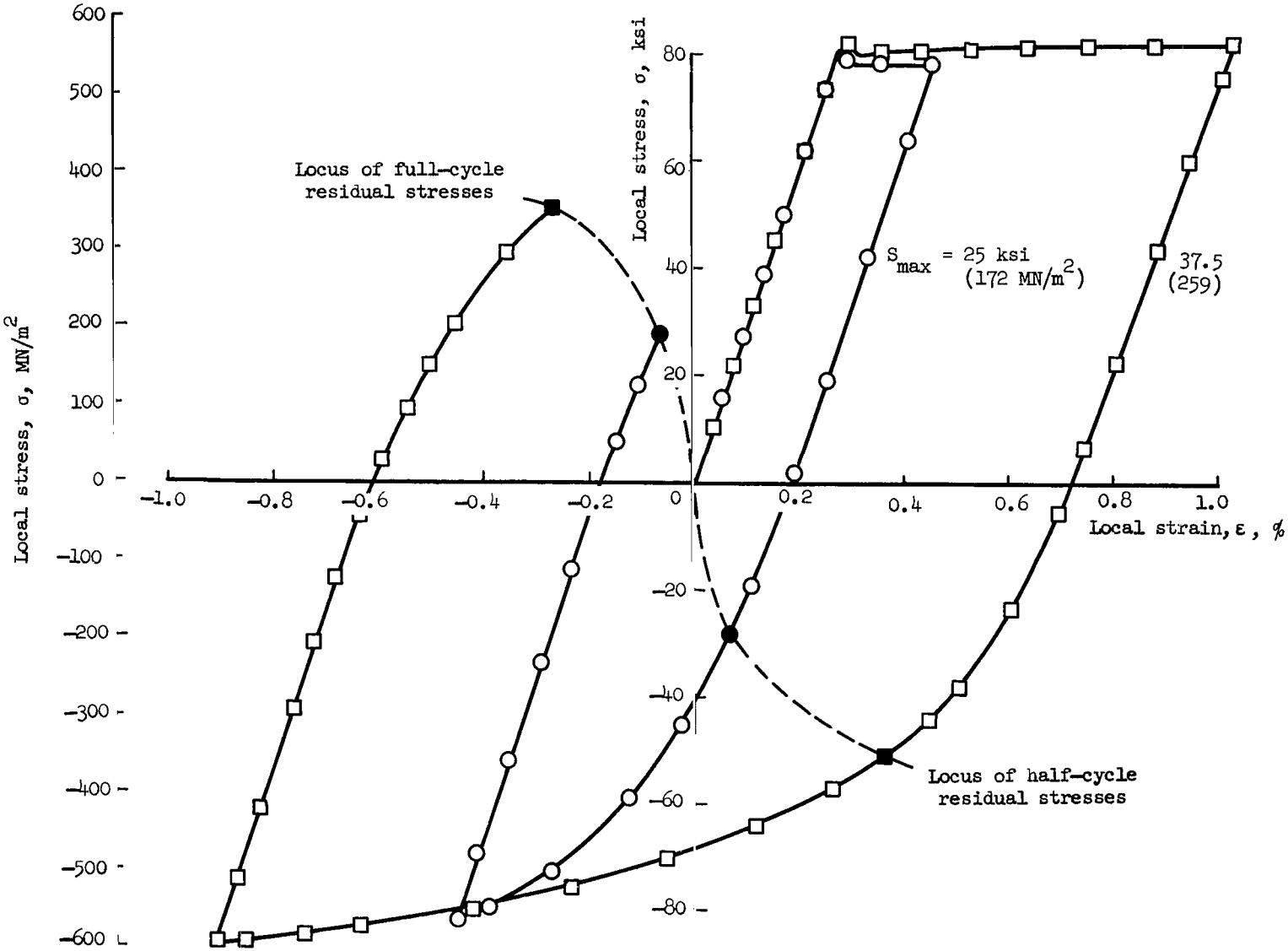

Figure 6.- Local stress-strain curves for first cycle. K_T = 4; AISI 4130 (normalized); R = -1. Solid symbols represent residual stress-strain values.

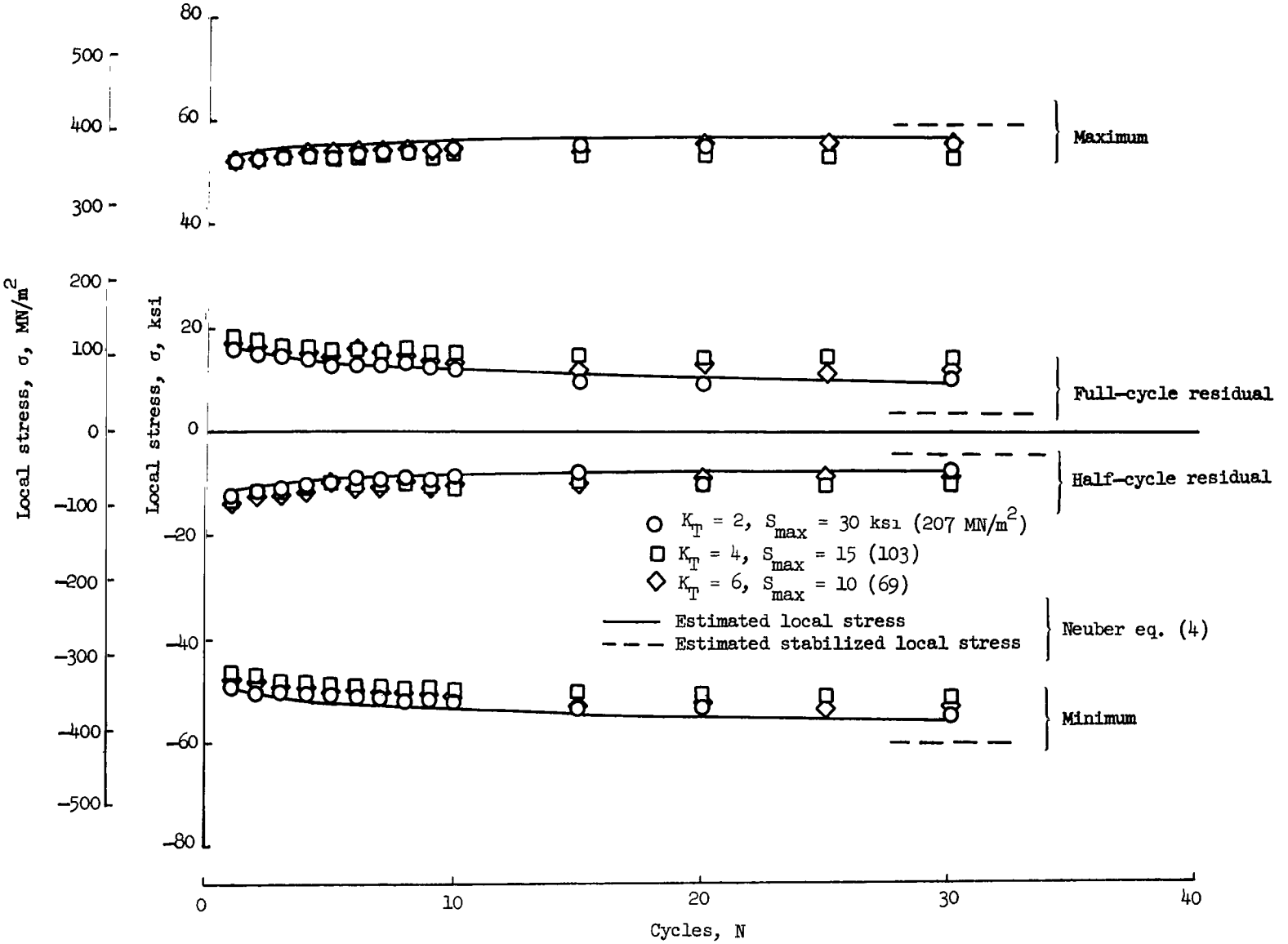

Figure 7.- Stabilization of experimental and estimated local stresses. $K_T S_{max}$ = 60 ksi (413 MN/m^2); 2024-T3; R = -1.

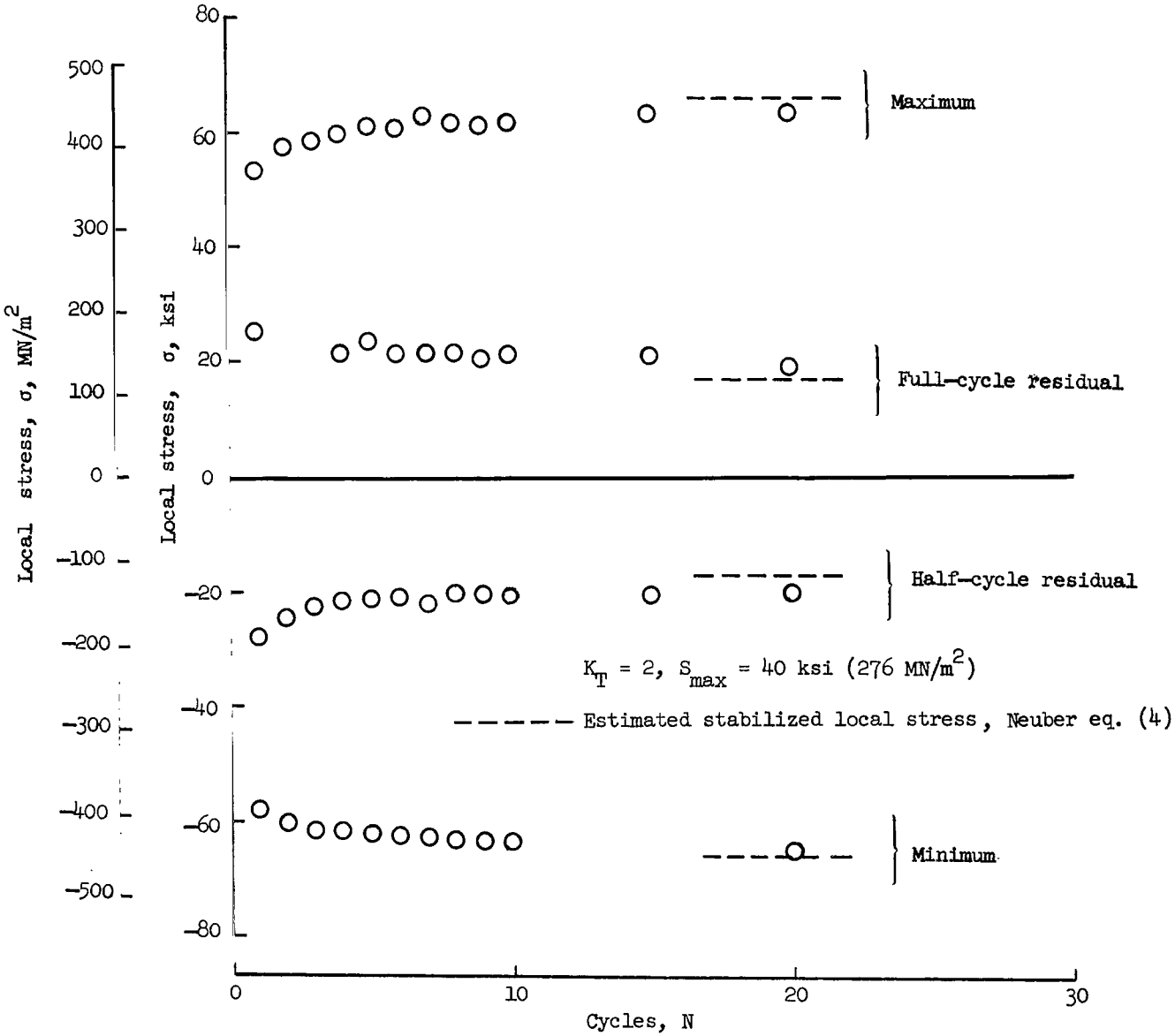

Figure 8.- Stabilization of experimental local stresses. $K_T S_{max}$ = 80 ksi (552 MN/m2); 2024-T3; R = -1.

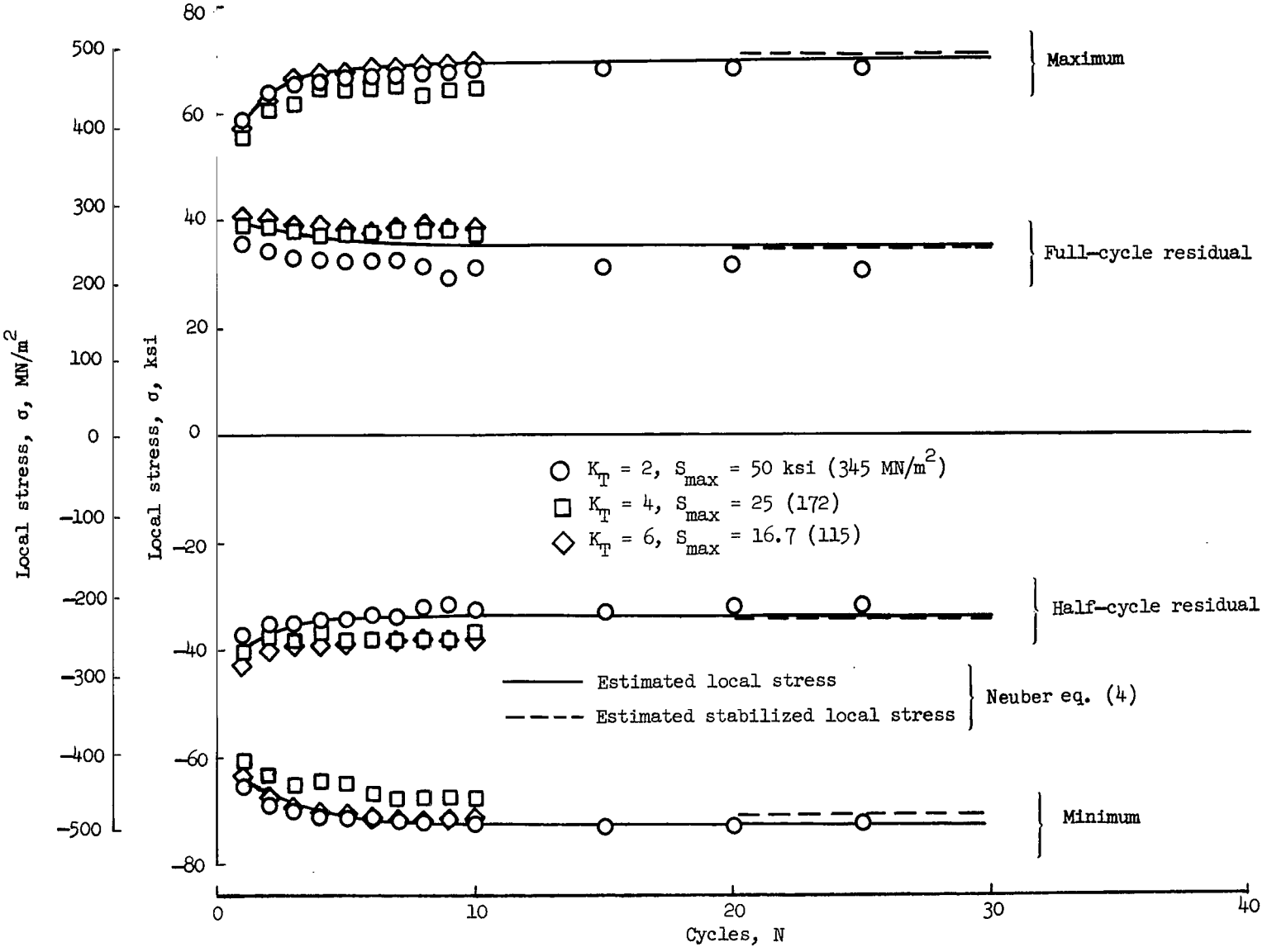

Figure 9.- Stabilization of experimental and estimated local stresses. $K_T S_{max}$ = 100 ksi (689 MN/m2); 2024-T3; R = -1.

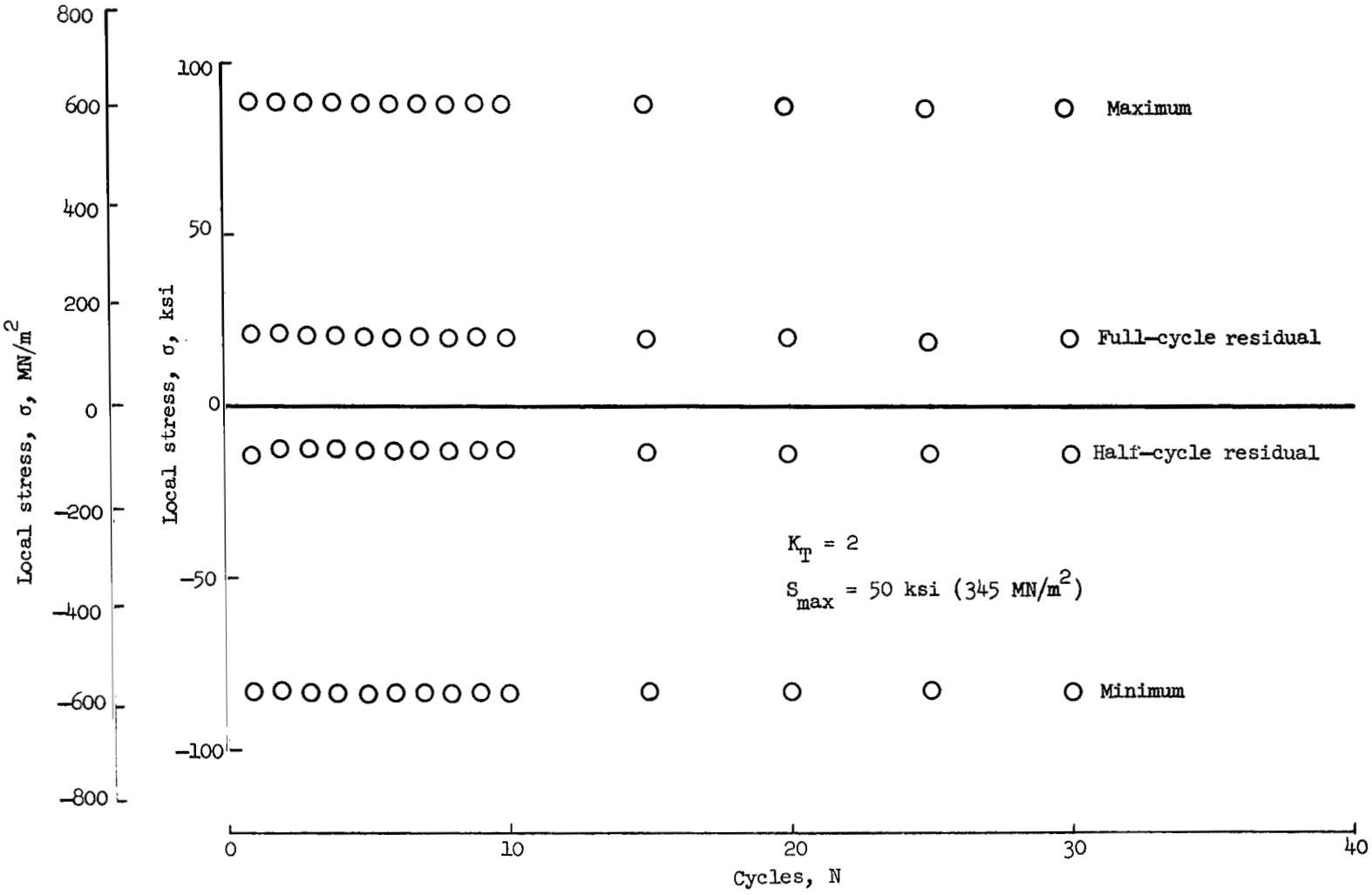

Figure 10.- Stabilization of experimental local stresses. $K_T S_{max}$ = 100 ksi (689 MN/m^2); SAE 4130 (normalized and stress relieved); R = -1.

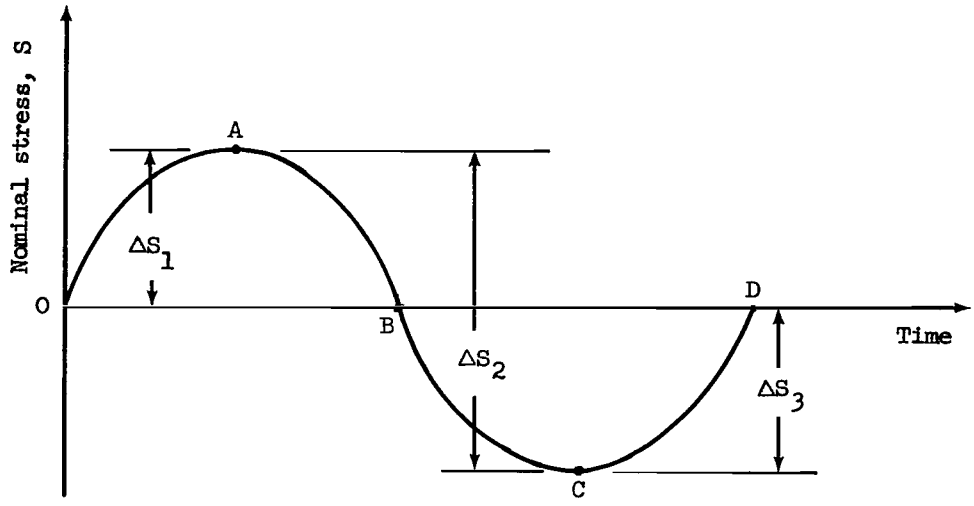

(a) Nominal stress cycle.

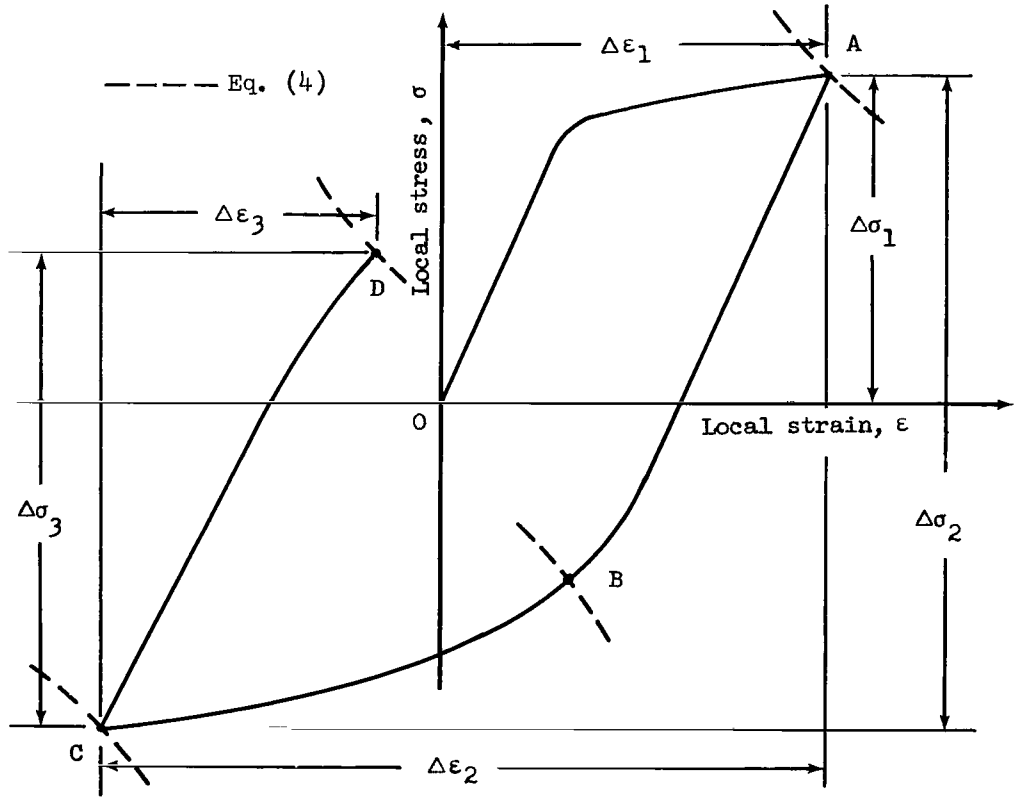

(b) Estimated local stress-strain curve.

Figure 11.- Nominal loading and estimated local stress-strain curve for the first loading cycle.

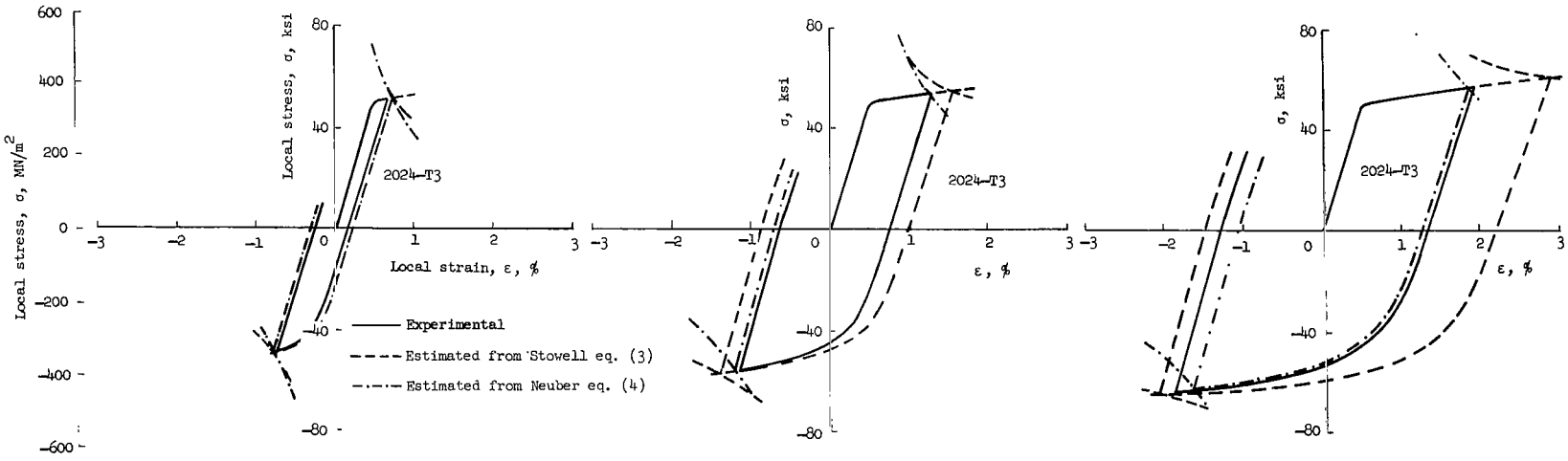

(a) $K_T = 2$, $K_{exp} = 2.12$, $S_{max} = 30$ ksi (207 MN/m^2). (b) $K_T = 2$, $K_{exp} = 2.12$, $S_{max} = 40$ ksi (276 MN/m^2). (c) $K_T = 2$, $K_{exp} = 2.09$, $S_{max} = 50$ ksi (345 MN/m^2).

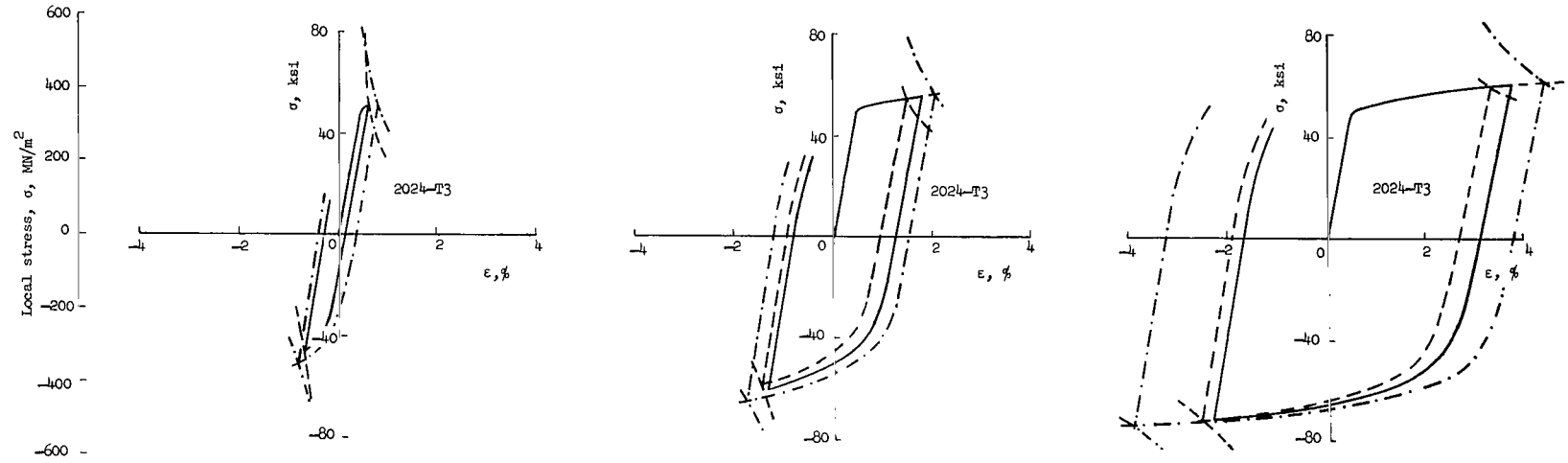

(d) $K_T = 4$, $K_{exp} = 4.39$, $S_{max} = 15$ ksi (103 MN/m^2). (e) $K_T = 4$, $K_{exp} = 4.46$, $S_{max} = 25$ ksi (172 MN/m^2). (f) $K_T = 4$, $K_{exp} = 4.54$, $S_{max} = 37.5$ ksi (259 MN/m^2).

Figure 12.- Comparison of estimated and experimental local stress-strain curves.

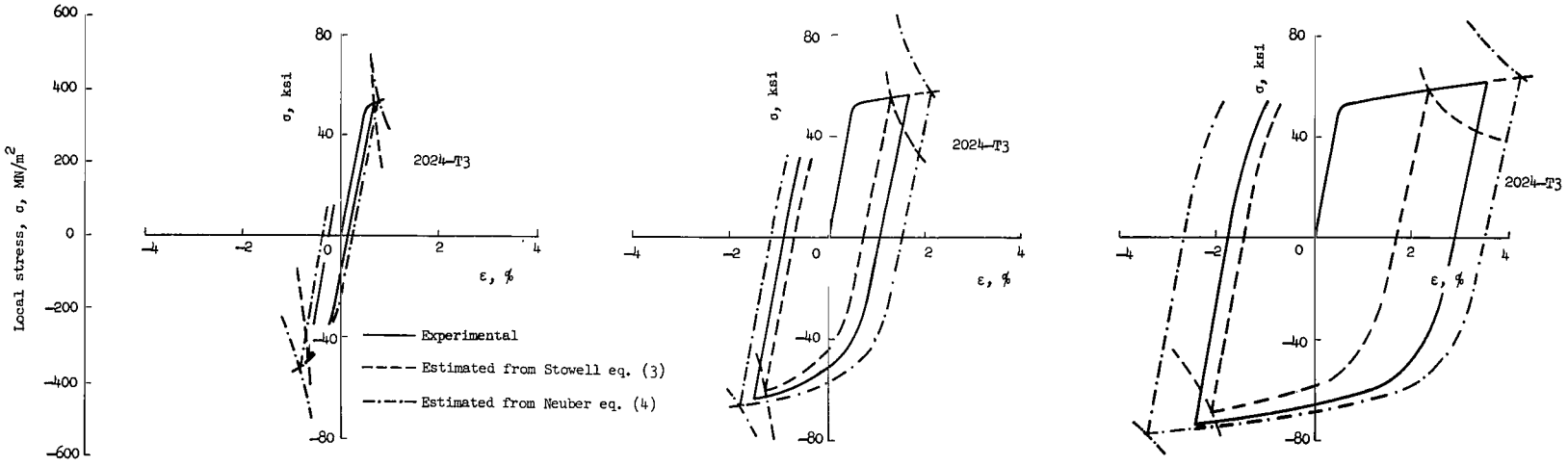

(g) $K_T = 6$, $K_{exp} = 6.68$, $S_{max} = 10$ ksi (69 MN/m^2). (h) $K_T = 6$, $K_{exp} = 6.82$, $S_{max} = 16.7$ ksi (115 MN/m^2). (i) $K_T = 6$, $K_{exp} = 6.77$, $S_{max} = 25$ ksi (172 MN/m^2).

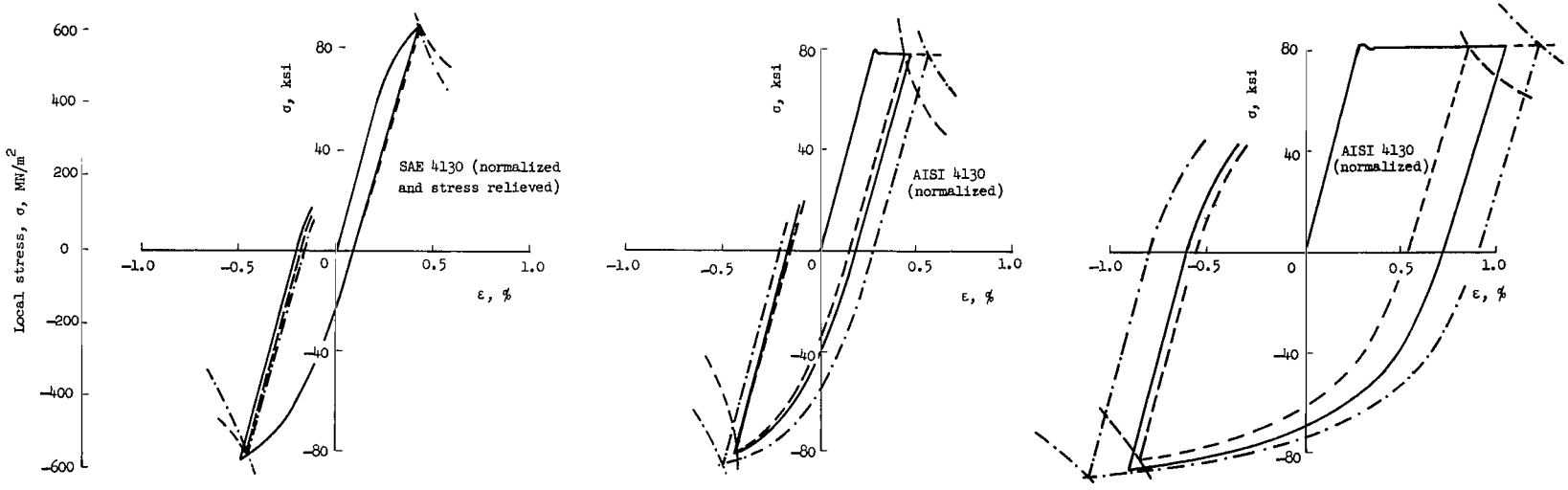

(j) $K_T = 2$, $K_{exp} = 2.08$, $S_{max} = 50$ ksi (345 MN/m^2). (k) $K_T = 4$, $K_{exp} = 4.50$, $S_{max} = 25$ ksi (172 MN/m^2). (l) $K_T = 4$, $K_{exp} = 4.56$, $S_{max} = 37.5$ ksi (259 MN/m^2).

Figure 12.- Concluded.

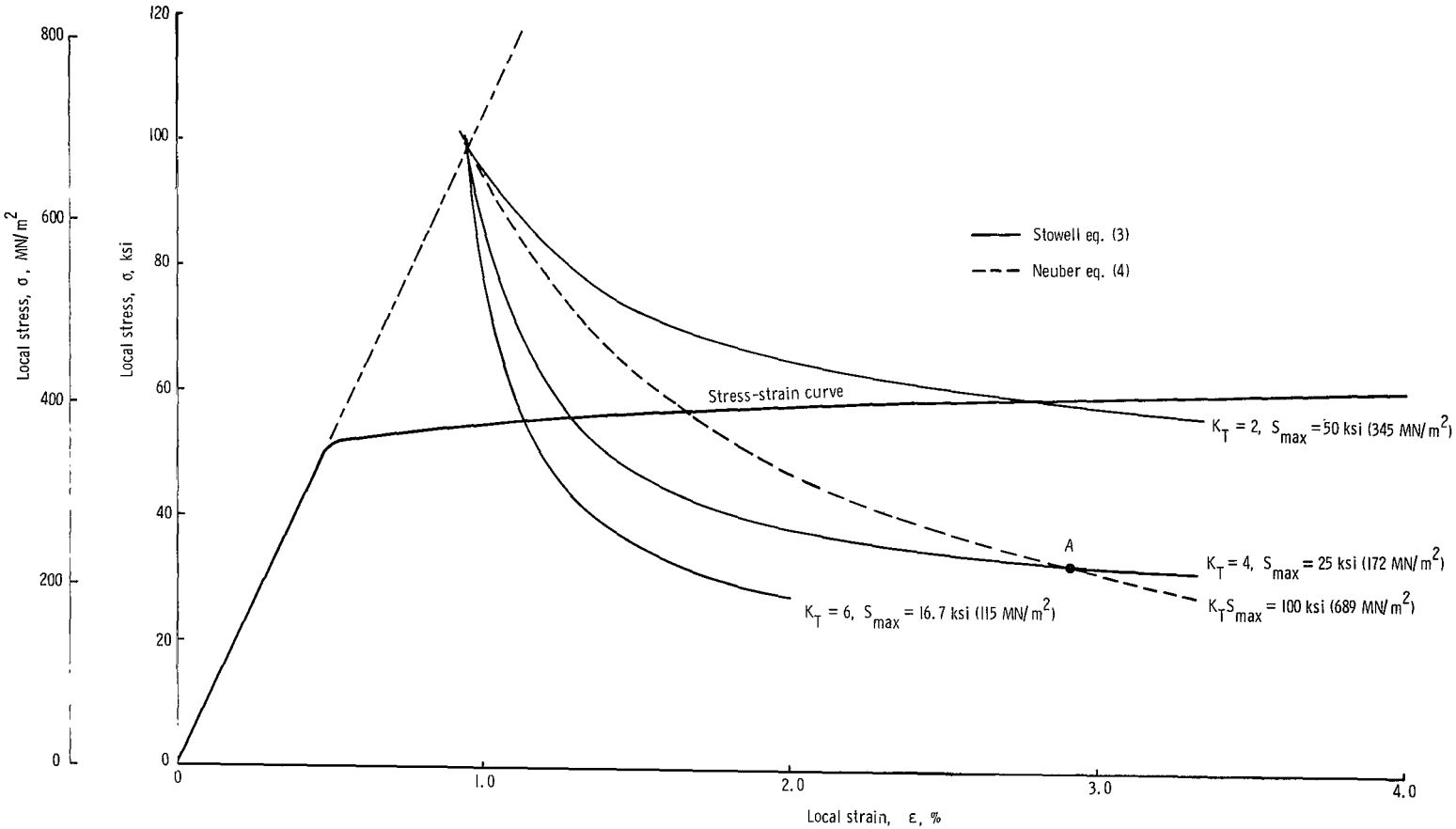

Figure 13.- Graphical comparison of Neuber and modified Stowell equations.

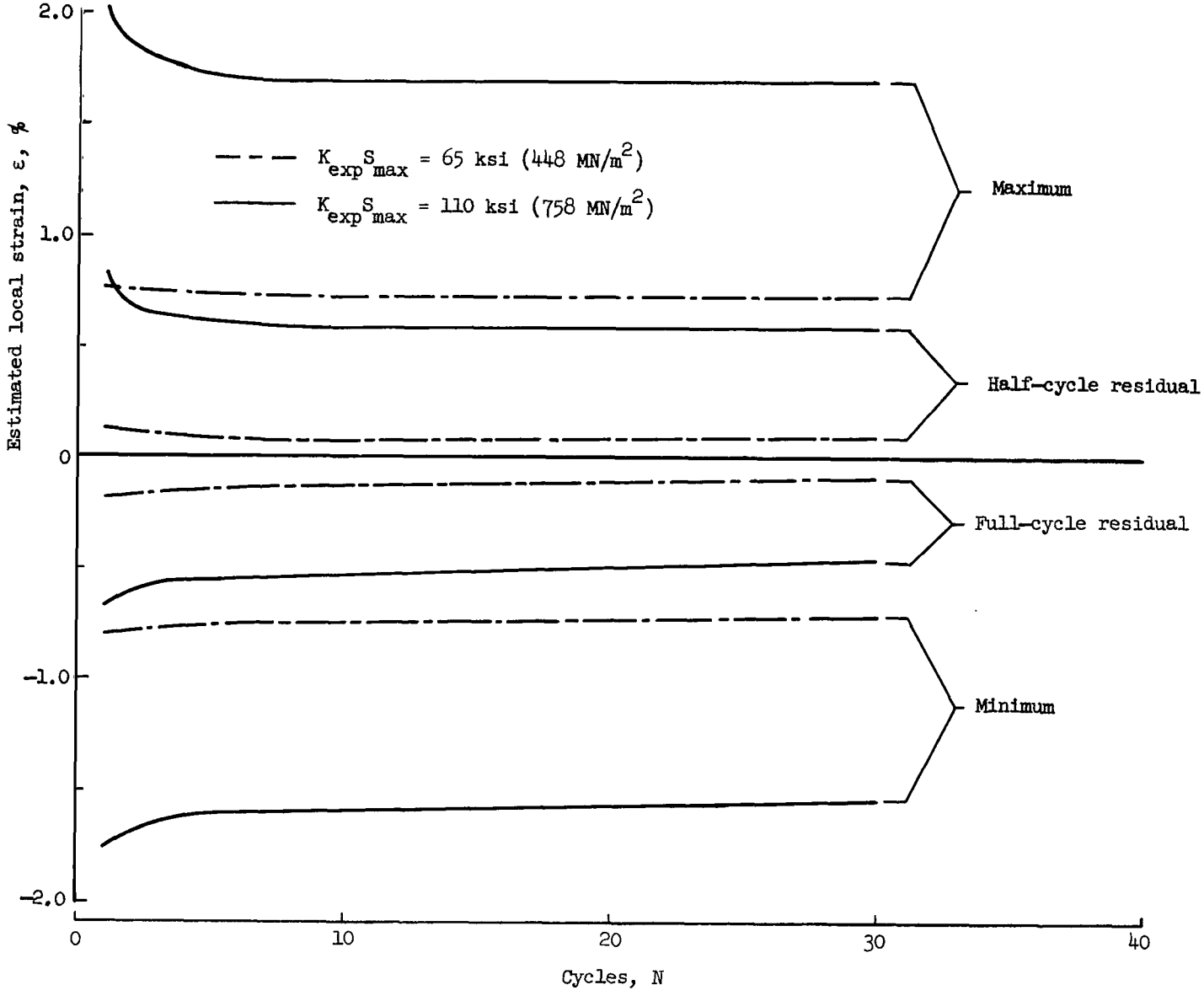

Figure 14.- Estimated local strain histories for 2024-T3.

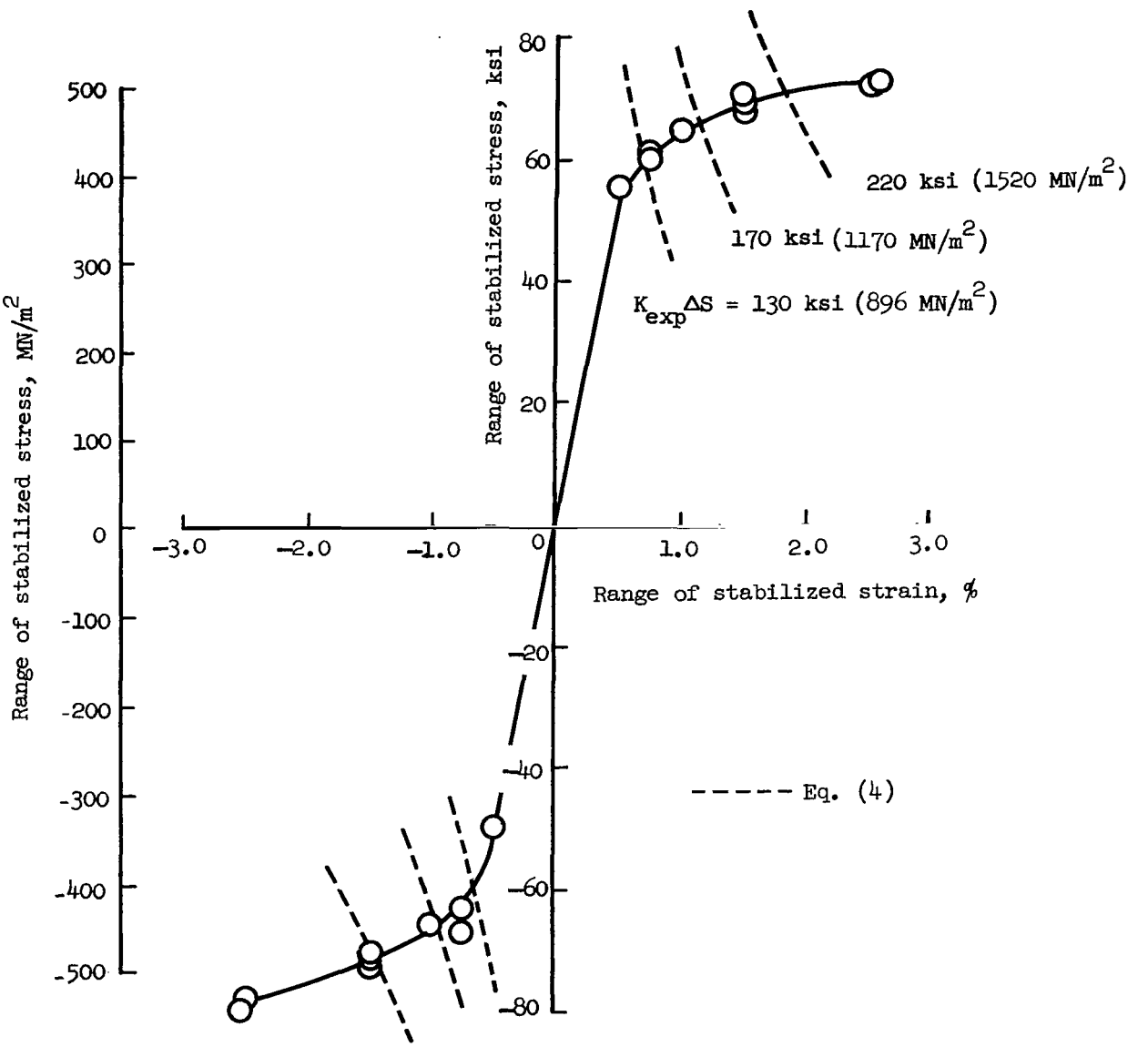

Figure 15.- Cyclic stress-strain curve for 2024-T3.

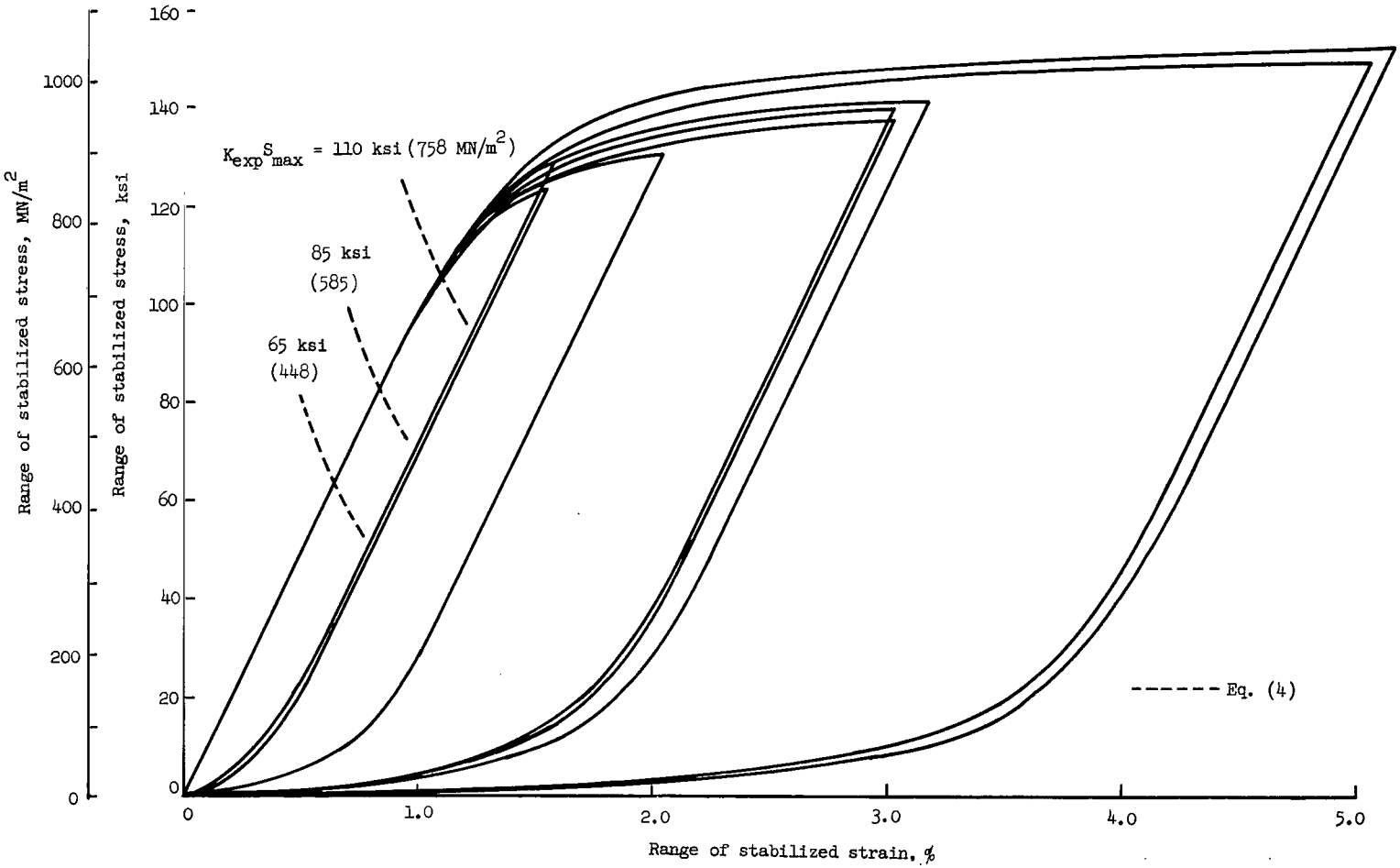

Figure 16.- Stabilized hysteresis loops for 2024-T3.

NATIONAL AERONAUTICS AND SPACE ADMINISTRATION
WASHINGTON, D. C. 20546

OFFICIAL BUSINESS

FIRST CLASS MAIL

POSTAGE AND FEES PAID
NATIONAL AERONAUTICS AND
SPACE ADMINISTRATION

POSTMASTER: If Undeliverable (Section 158 Postal Manual) Do Not Return

"The aeronautical and space activities of the United States shall be conducted so as to contribute . . . to the expansion of human knowledge of phenomena in the atmosphere and space. The Administration shall provide for the widest practicable and appropriate dissemination of information concerning its activities and the results thereof."

—NATIONAL AERONAUTICS AND SPACE ACT OF 1958

NASA SCIENTIFIC AND TECHNICAL PUBLICATIONS

TECHNICAL REPORTS: Scientific and technical information considered important, complete, and a lasting contribution to existing knowledge.

TECHNICAL NOTES: Information less broad in scope but nevertheless of importance as a contribution to existing knowledge.

TECHNICAL MEMORANDUMS: Information receiving limited distribution because of preliminary data, security classification, or other reasons.

CONTRACTOR REPORTS: Scientific and technical information generated under a NASA contract or grant and considered an important contribution to existing knowledge.

TECHNICAL TRANSLATIONS: Information published in a foreign language considered to merit NASA distribution in English.

SPECIAL PUBLICATIONS: Information derived from or of value to NASA activities. Publications include conference proceedings, monographs, data compilations, handbooks, sourcebooks, and special bibliographies.

TECHNOLOGY UTILIZATION PUBLICATIONS: Information on technology used by NASA that may be of particular interest in commercial and other non-aerospace applications. Publications include Tech Briefs, Technology Utilization Reports and Notes, and Technology Surveys.

Details on the availability of these publications may be obtained from:

SCIENTIFIC AND TECHNICAL INFORMATION DIVISION

NATIONAL AERONAUTICS AND SPACE ADMINISTRATION

Washington, D.C. 20546